# Direct measurement of the ionization source rate and closure of the particle balance in a helicon plasma using laser induced fluorescence.

Jonathan Green and Oliver Schmitz<sup>1</sup>

Engineering Physics Department, University of Wisconsin - Madison.

A detailed study of the flows of ion and neutral argon populations in a helicon plasma was carried out. Understanding the principle ion sinks and sources of neutral fueling is essential to understanding the ability of helicon wave heating to create high density plasmas. This heating mechanism and the neutral fueling required to sustain it and perhaps maniupulate the axial density profile in long cylindrical plasmas is an active research topic for advanced plasma wakefield accelerator concepts. Using laser induced fluorescence (LIF) of ion and neutral argon species, an ion flux of up to  $2.5 \times 10^{21} \text{ m}^{-2} \text{s}^{-1}$  was measured leaving the core of a helicon plasma with a peak electron density of  $4.0 \times 10^{18} \text{ m}^{-3}$ . Taking the divergence of the axial ion flux profile yields a minimum ionization rate estimate of  $2 \times 10^{21} \text{ m}^{-3} \text{s}^{-1}$ , and including the radial divergence increases the estimated ioniztion rate to approximately  $10^{22} \text{ m}^{-3} \text{s}^{-1}$ . Neutral flow velocities measured using LIF reveal a circulatory fueling and loss mechanism with distinct zones where radial or axial sources and sinks dominate.

## I. INTRODUCTION

Heating a plasma with radiofrequency (RF) electromagnetic waves in the helicon regime is an attractive method for producing high density, low temperature plasmas. Electron densities as high as  $10^{20}$  m<sup>-3</sup> have been achieved in helicon sources using only a few 10s of kilowatts of power<sup>1,2</sup>. The efficiency with which helicon waves can convert RF power into electron density is both its most sought after and poorly understood property. The ultimate density achieved in helicon plasma sources is tightly coupled to both the power and particle balance present during the discharge. In particular, the observation of neutral depletion underscores the importance of the particle balance<sup>3,4</sup>. In trying to explain the neutral depletion, multiple hypotheses have been proposed to explain the transport processes in effect. Chen et al have suggested electron ion pairs are predominantly lost radially and that axial losses are negligible<sup>5</sup>. Similarly Magee et al concluded that the depletion of neutrals in helicon plasmas was due to expulsion, e.g. by collisional processes, not simply ionization alone<sup>4</sup>. Despite multiple theories regarding the transport processes taking place, only a few studies have been done to study the flows present, definitively conclude whether axial or radial losses dominate, and identify the source and sink terms of neutral particles<sup>6,7</sup>. Answering these questions is the focus of this work.

To better understand the ionization source strength and distribution, laser induced fluorescence (LIF) was used to measure spatially resolved ion and neutral fluxes in the MARIA helicon device at several axial and radial locations. From these fluxes, a clear picture of the ion and neutral flow dynamics can be attained. Additionally, taking the divergence of the flux yields a direct measurement of the ionization source strength and distribution. While these measurements do not answer the question of how the RF wave energy is converted into electron-ion pairs, it represents the best observation of the actual ionization source distribution which is itself a direct result

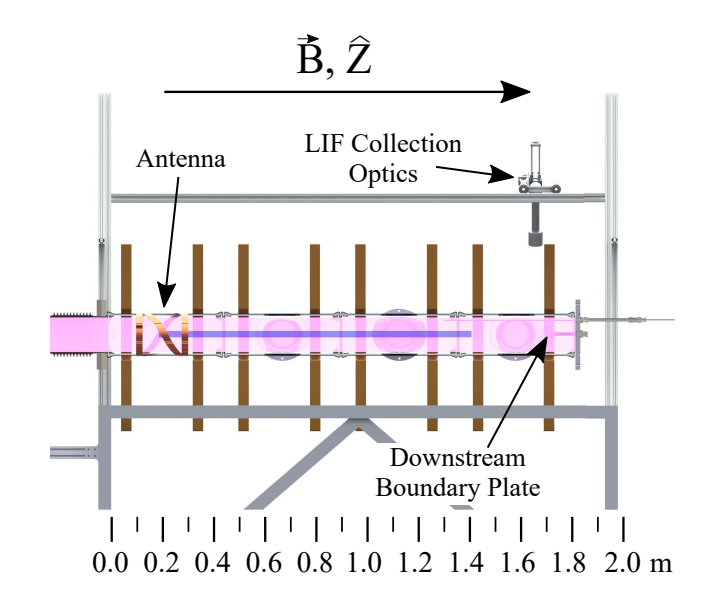


FIG. 1. Caption

of the RF to ionization coupling mechanism.

## II. EXPERIMENTAL APPARATUS

The measurements presented in this work were taken on the MARIA helicon device, shown in Figure 1, in the 3DPSI group at the University of Wisconsin - Madison<sup>8</sup>. MARIA is 2.4 m long with an inner chamber diameter of 14 cm. The antenna is an 18 cm long helical antenna designed to couple to the m=+1 mode. The magnetic field is generated by 8 water cooled pancake magnets and generates a peak magnetic field strength of 1005 G at 984 A of total current. A water-cooled solid state RF generator provides up to 10 kW of RF power and is typically operated at constant power (CW). A single RF compensated Langmuir probe, of the same type proposed by Chen  $et\ al^9$ , is the baseline diagnostic for electron tem-

perature and density measurements. Electron densities in the range of  $5 \times 10^{18}$  m<sup>-3</sup> are typical at neutral pressures in the range of 2 mTorr, with 700 W of RF power, and a magnetic field strength of 700 G.

The LIF system follows the master oscillator power amplifier (MOPA) design championed by Severn  $et~al^{10}$ , and is designed around a 40 mW tunable single mode diode laser and a tapered amplifier which can produce 500 mW of maximum laser power. This system can be tuned to pump the  $3d^4F$  7/2 to  $4p^4D5/2$  singly ionized argon absorption transition at 668.614 nm, or the  $4s^2[3/2]$  1 to  $4p^2[1/2]$  0 neutral argon absorption transition at 667.912 nm. The ion and neutral pumping strength, which is proportional to the density of atoms in the lower atomic level and incident laser power, is monitored via the fluorescence intensity at 442.6 nm and 750.6 nm respectively. More details of the LIF system and the typical analysis steps to extract flow measurements are provided in a paper by Green  $et~al^{11}$ .

Acylindrical coordinate system is adopted with the  $\hat{z}$  axis colinear with the chamber axis and parallel to the magnetic field as indicated in Figure 1. The 'downstream' direction is in the direction of the magnetic field. This direction points away from the antenna towards the blind end of the chamber. The reference point for axial position measurements is a part of the structure supporting the LIF collection optics. The center of the 18 cm antenna is located at 21 cm and the downstream plasma boundary is located at 168.4 cm. Positive and negative flow velocities discussed in this work match the coordinate system, i.e. 'positive' axial flow velocity is a flow in the +Z direction.

## III. THEORY

In this work, the source and sink terms of the mass conservation equation are the quantities of interest. By operating the plasma CW, the temporal component of the conservation equation can be neglected and the mass conservation equation simply balances the particle source and flux divergence,

$$\nabla \cdot (\mathbf{V}n) = S(\mathbf{x}). \tag{1}$$

Here **V** is the flow velocity, n is the number density, and S(x) is the ionization rate.

No particle flux variation is expected in the tangential direction of the coordinate system discussed previously. Separating Equation 1 into it's axial and radial components, and dropping the tangential component, yields

$$\frac{1}{r}\frac{\partial}{\partial r}(rnV_r) + \frac{\partial(nV_z)}{\partial z} = S(\mathbf{x}). \tag{2}$$

Here,  $V_z$  and  $V_r$  are the axial and radial flow velocity components respectively, and r is the radial position.

It is clear that an ionization source results in a positive value of flux divergence. Negative terms are indicative of an ion sink. The objective then is to measure the

particle flux,  $\Gamma = Vn$ , in both the radial and axial directions and calculate the divergence, thereby measuring the ion source and sink rate. By measuring the Doppler shift of the velocity distribution function using the LIF system, the flow velocity,  $\mathbf{V}$ , can be measured directly. However, the LIF intensity itself only yields information about the density of the atomic state being pumped. For determining the ionization source rate for a singly ionized ion population the total ion density is the desired quantity. In principle, a collisional radiative model might be used to infer total ion density and thus total electron density. However, failure to accurately capture all the relevant atomic processes in a collisional radiative model would make it quite difficult to interpret the results. In this work an empirical calibration between singly ionized argon LIF intensity and electron density is made from experimental measurements directly.

The minimum flow velocity uncertainty is limited by the absolute laser wavelength uncertainty. Previously the wavelength of a molecular iodine transition near 668.614 nm was reported as 668.6144 nm by Keesee et  $al^{12}$ , 668.6126 nm by Woo et  $al^{13}$ , and 668.6128 nm by Green et  $al^{11}$ . The wavelength of this iodine peak was further refined in this work by identifying the offset from the v = 0 transition wavelength of the  $3d^4F$  7/2 to  $4p^4D5/2$  singly ionized argon absorption transition. The v=0 wavelength was identified using LIF spectra simultaneously captured using forward and back propagated laser beams. The refined wavelength of 668.61272  $\pm 3.13 \times 10^{-5}$  nm was found from the standard error of the mean of 7 measurements. The uncertainty of the 668.614 nm transition was taken from Whaling et  $al^{14}$ , which itself is the source of the data held in the NIST ASD database<sup>15</sup>.

The prominent I<sub>2</sub> peak near the 667.9125 nm Ar I transition was measured in a similar way. Unfortunately the very low flow velocity meant that the  $\mathbf{k} \cdot \mathbf{V}$  and  $-\mathbf{k} \cdot \mathbf{V}$ components were not sufficiently separated to follow an analysis procedure identical to the argon ion transition. Instead the laser was passed through the plasma radially such that the beam could be reflected off an external mirror for the second, counter propagating, pass through the plasma. One set of data was taken with laser beam dump in place of the mirror such that the  $\mathbf{k} \cdot \mathbf{V}$  component is first acquired. This is plotted as the red trace in Figure 2. The beam dump is then replaced with a mirror and an LIF signal with the forward and backward component is acquired; the teal trace in Figure 2. The red trace can then be subtracted from the teal trace to reveal the  $-\mathbf{k} \cdot \mathbf{V}$ , plotted as the black dash-dot trace. The midpoint between the  $\mathbf{k} \cdot \mathbf{V}$  and  $-\mathbf{k} \cdot \mathbf{V}$  curves which corresponds to the V = 0 transition frequency of 667.9125 provided by NIST could then be identified. The uncertainty in the 667.9125 nm line was taken from Whaling  $et \ al^{16}$ .

The wavelength of the  $I_2$  peak near 667.9125 nm was determined in the same way as the 668.6128 nm line, with multiple samples. The final value of 667.91687  $\pm$ 

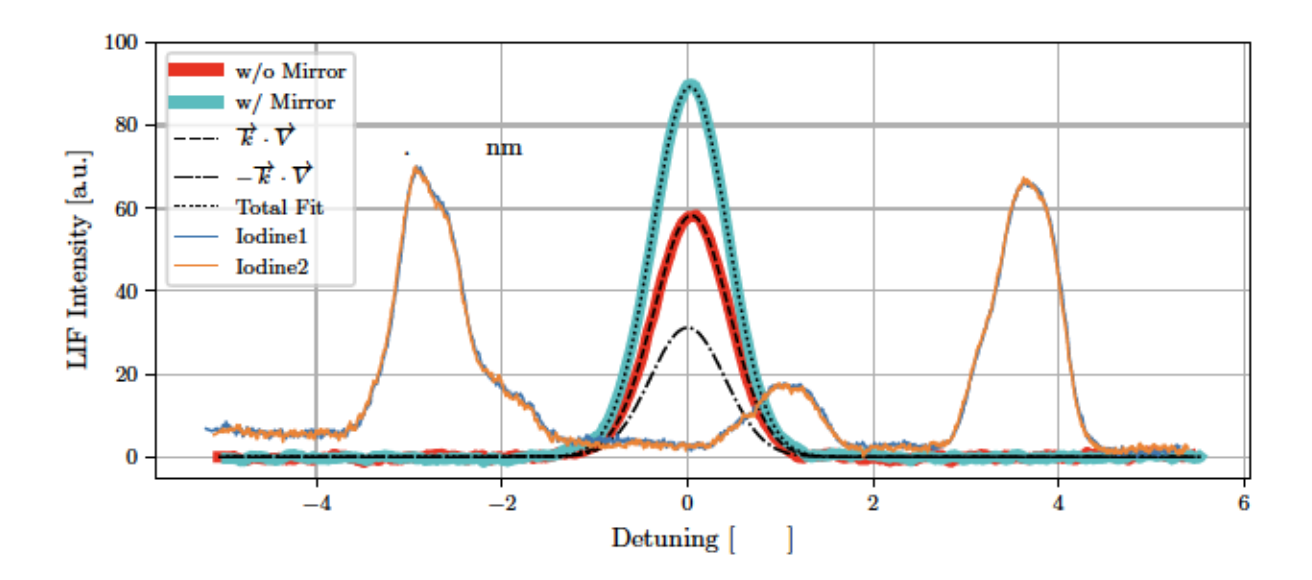


FIG. 2. The molecular iodine absorption peak indicated as 667.91687 nm at -2.9 GHz was identified by finding the v=0 midpoint between the  $\mathbf{k} \cdot \mathbf{V}$  (dashed line) and  $-\mathbf{k} \cdot \mathbf{V}$  (dash-dot line).

 $3.10 \times 10^{-5}$  nm was found from the standard error of the mean of 8 measurements.

It is important to note, that the I<sub>2</sub> peak wavelengths were essentially calculated as offsets from well known argon lines. The minimum uncertainty in the I<sub>2</sub> wavelength is then at least as large as the wavelength uncertainty of the argon line to which it is compared. This lower limit leads to a minimum velocity uncertainty of 17 m/s and 11 m/s for the neutral and singly ionized argon species respectively.

#### IV. RESULTS

# A. LIF to Electron Density Calibration

To correlate the LIF intensity with the electron density, LIF measurements were made at the center of the plasma at the same location as the Langmuir probe. The magnetic field strength was then scanned over the same range as was used for the measurements presented below. Plotting the electron density as a function of LIF intensity, shown in Figure 3 for both the axial and radial case, yields the scaling required to infer electron density from LIF intensity measurements.

Ideally, both of the curves in Figure 3 would lie on top of each other. However, two differences combine to cause the radial data to be higher than the axial data. First, the axial and radial data were taken before and after a vacuum leak was fixed in the vacuum chamber. The plasma chamber itself was cleaned when the leak was repaired and likely resulted in better chamber conditioning leading to higher density. The optical arrangement for the axial vs radial measurement is significantly dif-

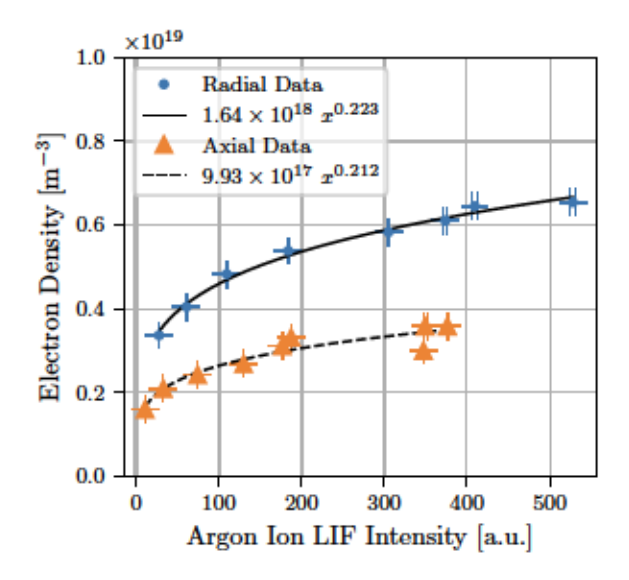


FIG. 3. Calibration curve for converting singly ionized argon LIF intensity to electron density. Here, the electron density is that measured by the RF compensated Langmuir probe. The LIF intensity was measured during the same discharge and at the same location as the Langmuir probe.

ferent. It is possible that the laser injection optics and fluorescence collection optics were not perfectly aligned for the radial case leading to lower apparent LIF intensity. Despite the opportunity for improvement, the same optical arrangement used during calibration was used for the measurement for both the axial and radial case.

# B. Argon Ion LIF

For the argon ion axial LIF data the laser was aligned with the axis of the chamber and the collection optics were traversed along the axis of MARIA, collecting fluorescence photons emitted perpendicular to the laser beam. The LIF spectra intensities were converted to electron density using the axial calibration data shown in Figure 3. The calculated electron density at several magnetic field strengths and plotted as a function of axial position along the plasma chamber is shown in Figure At magnetic field strengths below approximately 600 G, e.g. the 500 G trace, the electron density is relatively evenly distributed between the antenna and the downstream boundary plate. As the magnetic field strength is increased further, the electron density does not increase significantly near the antenna at 210 mm, and appears to hit an upper limit near 700 G at an axial location of 680 mm. Further downstream however, near 1200 mm, the electron density continues to increase with increasing magnetic field strength. The result of this asymmetric density scaling with magnetic field strength is a downstream shift in location of the maximum electron density. This shift suggests a change in the fueling and ionization equilibrium reached at different magnetic field strengths.

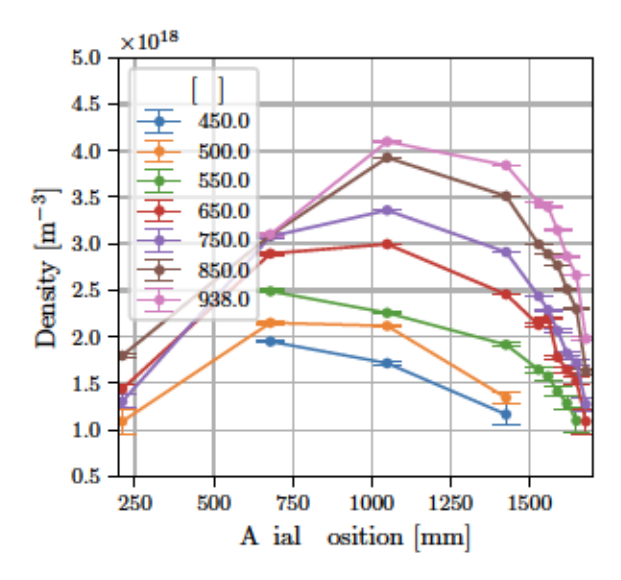


FIG. 4. The electron density found by scaling the singly ionized argon LIF intensity by the axial calibration data shown in Figure 3.

The argon ion flow velocity measurements, shown in Figure 5, are extracted directly from the LIF data by measuring the Doppler shift of the absorption spectrum. The flow velocity is negative near the antenna, crosses the horizontal axis at 900 mm, and transitions to a strong positive velocity near 1500 mm. Not much can be said about the cause from this data alone, but the sharp increase in velocity beyond 1600 mm is likely the velocity increase that occurs in the presheath to satisfy the Bohm criterion <sup>17</sup>. The sound speed for the 2.5 eV plasmas in this case is 2,461 m/s, and the closest measurement was approximately 4 mm from the sheath boundary. If this is indeed the case, the lack of any velocity scaling with magnetic field strength may indicate near constant electron temperature and thus constant ion sound speed.

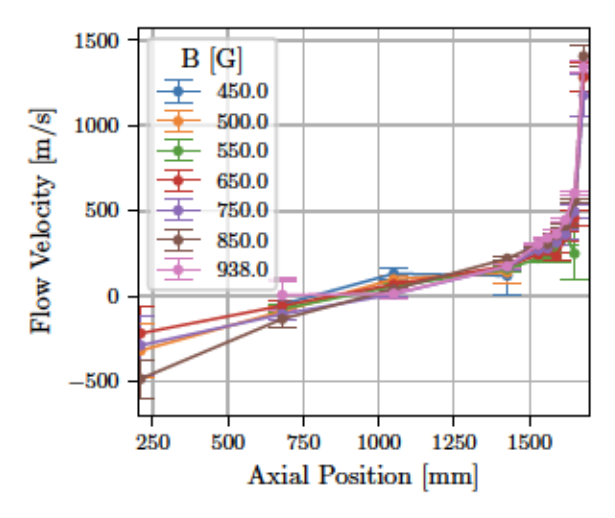


FIG. 5. The flow velocity of singly ionized argon atoms in the 3d <sup>4</sup>F 7/2 metastable state.

The shape of the axial ion flux profile shown in Figure 6, which is a product of the density and velocity data, is most strongly influenced by the ion velocity profile and thus has a very similar shape. The flux is negative (upstream flow) near the antenna, crosses the horizontal axis near 900 mm, and transitions to a strong positive flux (downstream flow) near 1500 mm. The flux is augmented up or down depending on the electron density. Ignoring the exponential region likely due to the presheath, the slope of the ion flux measurements clearly suggests an ionization source distributed along the axis of the device.

Taking the divergence of just the axial flow data, the contribution of axial flux divergence to the ionization source rate can be determined. This data alone represents a lower bound for the ionization source rate. The divergence of the axial flux data is shown in Figure 7. The rapid flux increase in the presheath region near 1650 mm results in a significant ionization rate there. However, in the main plasma region between 450 mm and 1500 a distinctly positive ionization source rate of  $\sim 10^{21} \text{ m}^{-3}\text{s}^{-1}$ is also evident. Despite some scatter in the data, a fairly clear scaling with magnetic field strength is also evident at 1250 mm. This suggests an ionization rate that scales similarly to the helicon dispersion relationm, with a dependence on magnetic field strength. However the downstream shift in the location of maximum electron density can also affect the divergence calculation. A slight dip at

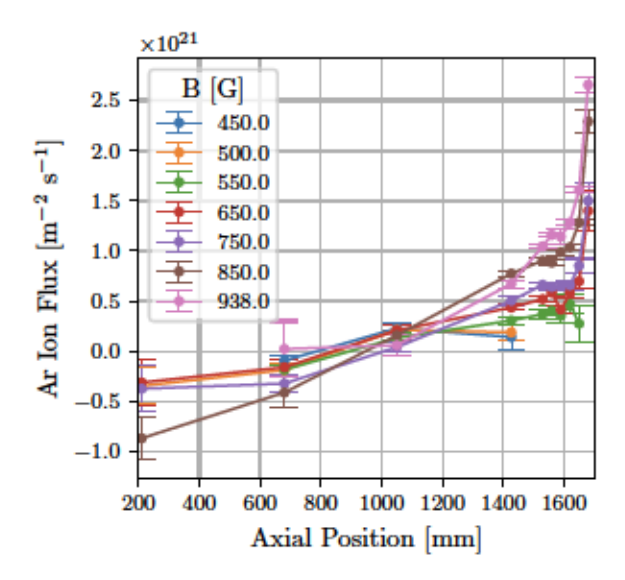


FIG. 6. The flux of singly ionized argon calculated by multiplying the electron density, Figure 4, with the ion flow velocity, Figure 5.

1650 mm in the ionization rate calculated from the axial data suggests an ion sink in this region. However, the radial contribution must be included before any conclusion regarding this possible sink is drawn.

The radial ion flux measured at radial positions of r/a  $\leq 0.05$ , r/a = 1/3, and r/a = 2/3, and the same axial locations as for the axial data are shown in Figure 8. At all positions there is a consistent outward radial flux on the order of  $2.5 \times 10^{20} \ \mathrm{m^{-2}s^{-1}}$  with slightly higher values at an axial position of 680 mm. Despite a fairly consistent flux, the density of ions in the 3d  $^4F$  7/2 state able to absorb laser photons was significantly lower at greater radii leading to decreased signal to noise ratio. Signals below a certain threshold could not be fit reliably and hence were not plotted in the figure leading to the sparsity of data points at r/a = 2/3. The radial flux between  $2.5-5\times10^{20} \ \mathrm{m^{-2}s^{-1}}$  is comparable to the axial flux measured between 680 mm and 1400 mm. This already means that over the bulk plasma domain, neither the axial nor radial flux dominates the loss channel.

It is also interesting to note that the perpendicular flux is comparable to Bohm-like diffusion. The Bohm diffusive flux, J, is calculated by  $J=D_B\,dn_e/dr$  and  $D_B=ckT_e/16eB$ , where c is the speed of light, k is Boltzman's constant,  $T_e$  is the electron temperature, B is the magnetic field strength, and e is the charge of an electron. Taking the density gradient in the radial direction from Langmuir probe measurements gives a radial flux between  $1-4\times10^{20}~\mathrm{m^{-2}s^{-1}}$ . This is the same conclusion reached by Rapp et~al after comparing the results of numerical simulations to experimental density data<sup>18</sup>. Taking LIF data with higher spatial resolution might be an even better comparison with the numerical data of Rapp et~al.

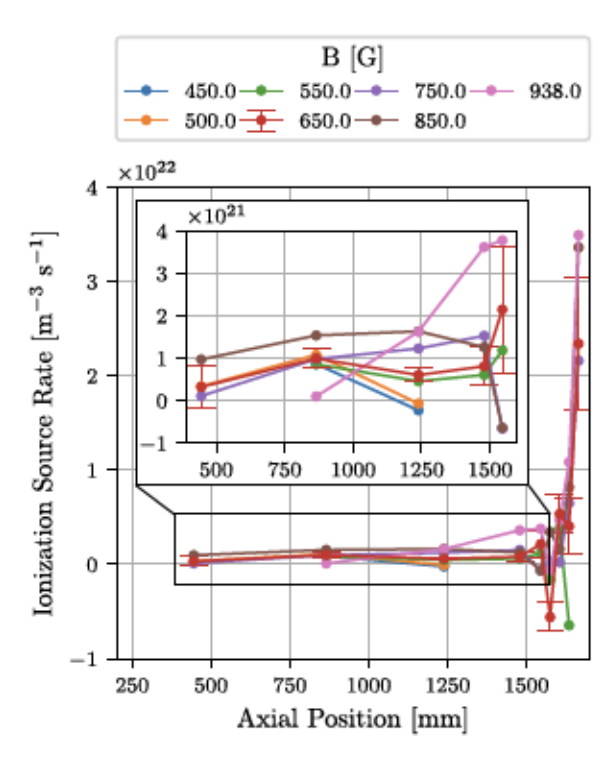


FIG. 7. The ionization source rate calculated by taking the divergence of the axial ion flux, shown in Figure 6. Typical uncertainties are indicated by the 650 G trace.

Calculating the contribution of the radial flux divergence to the ionization source rate is complicated by the sparse data. No differentiable radial trend can be identified to perform the necessary calculations. Assuming a constant flux yields an axially peaked ionization source, but one that blows up at r = 0 which is unphysical. Calculating an approximate flux gradient based on the r/a = 1/3 and r/a = 2/3 data, and assuming a linear trend between these two data points, yields an ionization source rate of 10<sup>22</sup> m<sup>-3</sup>s<sup>-1</sup>. However, this calculation carries an uncertainty of 200%. The ionization rate of 10<sup>22</sup> m<sup>-3</sup>s<sup>-1</sup> is comparable to the ionization rate calculated from the axial flux data in front of the boundary plate. This suggests a bulk plasma ionization rate between  $.5-1 \times 10^{22}$ m<sup>-3</sup>s<sup>-1</sup>. Higher spatial resolution in the radial direction is needed to better constrain the radial flux profile and ionization source rate.

### C. Neutral Argon LIF

Where there is an ion source via ionization in a singly ionized plasma, there must necessarily be a neutral sink. Fortunately the diode laser used in this work can be retuned to lase at 667.912 nm to pump the 4s <sup>2</sup>[3/2] 1 to 4p <sup>2</sup>[1/2] 0 neutral argon absorption transition. The neutral LIF intensity is directly proportional to the density

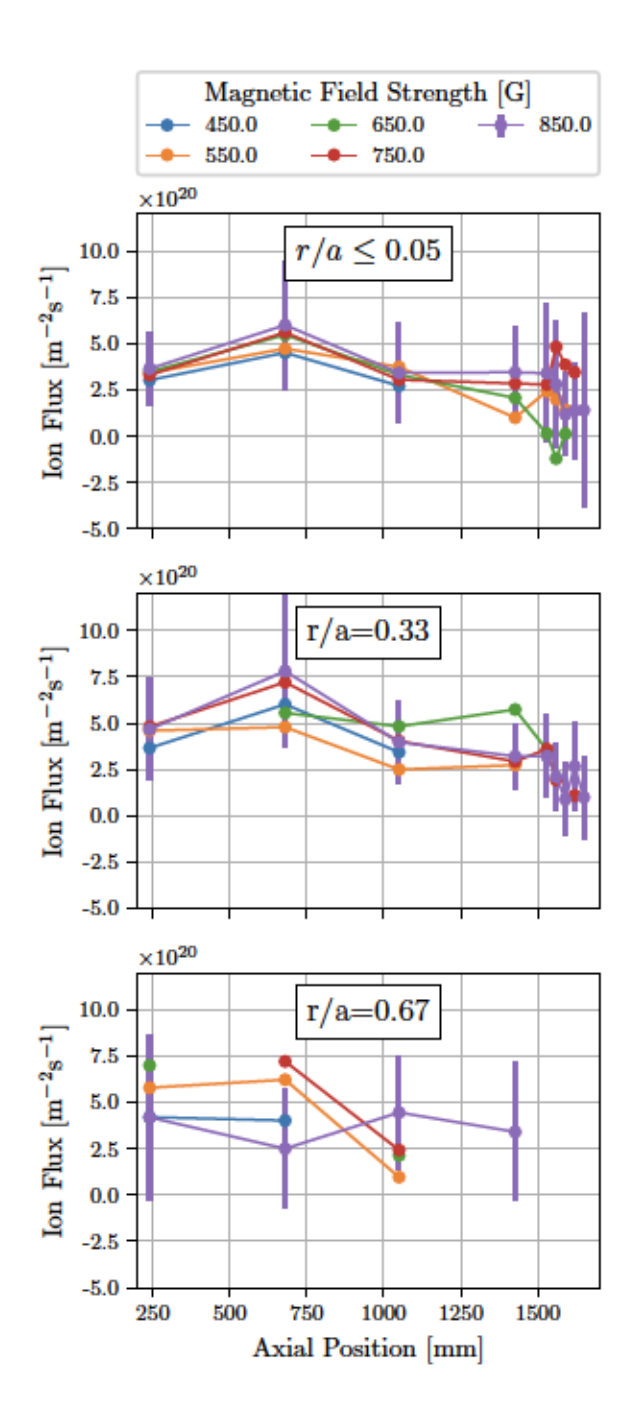


FIG. 8. Off axis radial argon ion LIF intensity measurements. Typical uncertainties are indicated by the 850 G trace.

of the 4s <sup>2</sup>[3/2] 1 excited atomic level of neutral argon. This level is directly populated from the neutral argon ground state via electron impact excitation. So, while it's connection to the neutral ground state makes it a decent measure of the ground state population, the level density is also very sensitive to the electron density. Unfortunately, no other diagnostics that could measure localized neutral densities were available to create an LIF signal to neutral density calibration. However, as shown below,

the mass conservation equation can be used to estimate the neutral atom density using the axial neutral argon LIF data alone.

The neutral argon intensity profile taken with the laser aligned along the axis of the device, shown in Figure 9A, is nearly an inverse of the ion density profile. This is generally expected as a high electron density suggests a high ionization rate and thus rapid conversion of neutrals into ions. At low magnetic field strength, ≤ 400 G, the neutral LIF intensity is fairly broad and extends along a significant length of the MARIA chamber. Between 500 G and 600 G or so the the neutral intensity profile increases and is concentrated near an axial position of 1400-1700 mm. However, below 1400 mm the neutral LIF intensity is significantly reduced indicating a reduced density of neutral atoms in that region. Above 600 G the neutral intensity is still concentrated in the same axial location, but the intensity decreases with further magnetic field strength increase.

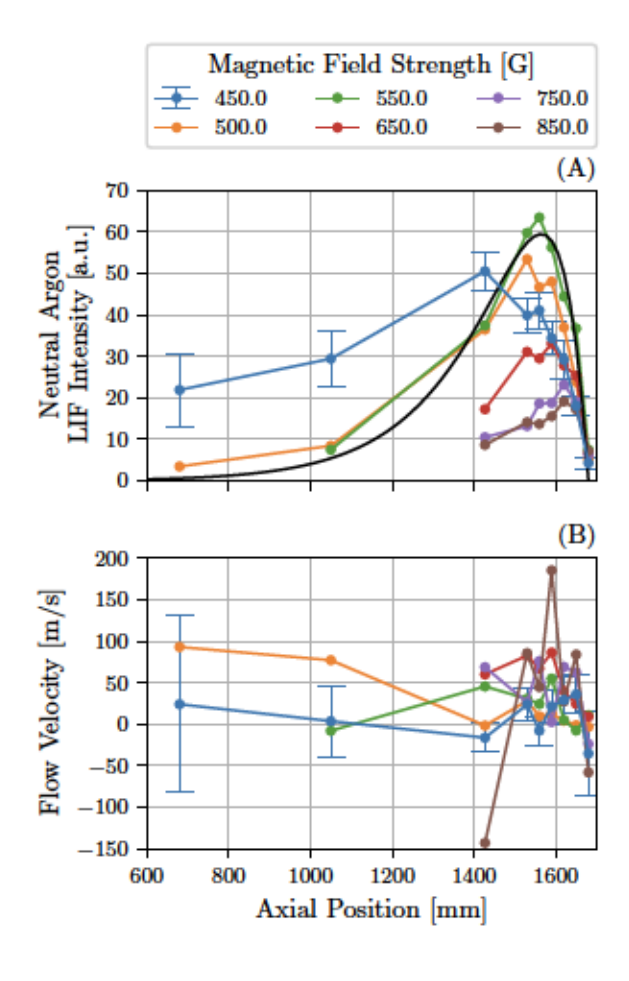


FIG. 9. A.) Neutral argon LIF intensity which is proportional to the 4s <sup>2</sup>[3/2] 1 atomic level density. The fit of Equation 4 to the 550 G trace is indicated by the black line. B.) Average flow velocity of neutral atoms in the 4s <sup>2</sup>[3/2] 1 excited level. Error bars are hidden for clarity but typical errors are shown on the 450 G trace.

The neutral flow velocities, shown in 9B, are much slower, around 50 m/s, in contrast to the argon ion flow velocities which exceeded 1000 m/s in the presheath region. The velocity measurement closest to the boundary plate at 1680 mm, which was 4 mm away from the plate, is negative for all magnetic field strengths. The flow velocity is positive between axial locations of 1400 and 1650 mm. Between 600 and 1400 mm the flow appears to be positive, but low signal to noise ratio means many data points are missing and data that could be analyzed carries larger uncertainty. The apparent flow velocity reversal is a curious feature that could support the theory of Magee et al that collisional neutral expulsion is playing a role in the bulk plasma neutral depletion.

The neutral intensity and flow velocity evolution is intuitive in the context of strong ion flux towards the boundary plate. Ions impinging on the boundary plate are neutralized and are necessarily recycled back into the plasma volume as neutral atoms. These recycled neutral atoms are then exposed to the flux of ions and electrons and can undergo ionization and experience collisional momentum transfer. The flow reversal is possibly an indication of the collisional momentum transfer, while the strong buildup and then decay of the LIF intensity is an indication of the electron impact excitation and ionization process.

By applying this hypothesis to the data, we find that a very simple two species exponential decay model fits the axial neutral LIF data quite well. The model used takes the form:

$$\frac{dn_1}{dz} = -\lambda_1 n_1,$$

$$\frac{dn_2}{dz} = -\lambda_2 n_2 + c\lambda_1 n_1,$$
(3)

which has the solution:

$$n_1 = n_0 \exp(-\lambda_1 z),$$
  
 $n_2 = \frac{c\lambda_1 n_0}{\lambda_2 - \lambda_1} (\exp(-\lambda_1 z) - \exp(-\lambda_2 z)).$  (4)

In this very simple model  $n_0$  is the ground state immediately adjacent to the downstream boundary plate,  $n_1$  represents the neutral argon ground state density,  $n_2$ is the density of the atomic level being pumped in the LIF process, and  $\lambda_1$  and  $\lambda_2$  are the decay constants for the two atomic levels respectively. The physical 'decay' mechanism within this model is electron impact excitation from level 1 to level 2 followed by further excitation and ionization from level 2. The factor c is a constant that takes into account the fact that not all excitation out of the ground level ends up in the single excited level. Insufficient data is available to fully constrain the value of c. However, recognizing that it is simply a density scalar for the 4s <sup>2</sup>[3/2] 1 neutral argon level, it's value can temporarily be set to an arbitrary value, c = 1 here, and the data can be fit remarkably well as indicated by the black line in Figure 9A.

TABLE I. Fitting parameter values optained from fitting Equation 4 to the neutral argon LIF data.

B-field [G]	$n_0$	$\lambda_1$	$\lambda_2$
450	$4.59\times10^{18}$	9.6	1.3
500	$7.15\times10^{18}$	9.7	5.0
550	$9.35\times10^{18}$	10.3	6.5
650	$1.63\times10^{19}$	4.8	21.8
750	$2.33\times10^{19}$	4.3	51.5
850	$4.33 \times 10^{19}$	3.3	95.1

Despite setting c = 1 in this work, reasonable estimates of the neutral argon ground state density near the boundary plate can be made. As described above, the flux of ions into the boundary plate must reappear as a flux of neutral atoms. To calculate the flux, a recycling velocity must be determined. Unfortunately the neutral velocity is pretty scattered, but the average recycling velocity for all mangetic field strengths 4 mm in front of the plate was 25 m/s away from the plate. Multiplying the values of  $n_0$  found through fitting Equation 4 to each of the traces in Figure 9A and matching to the argon ion flux in Figure 6 indicates  $n_0$  should be scaled by  $7.2 \times 10^{16}$  to yield the neutral argon flux in m<sup>2</sup>/s. The ion and neutral particle flux in close proximity to the boundary plate at each magnetic field strength after scaling  $n_0$  is shown in Figure 10. The agreement between the two is very good, and both scale with increasing density as expected. A table showing the values obtained by fitting Equation 4 to the LIF data is shown in Table I.

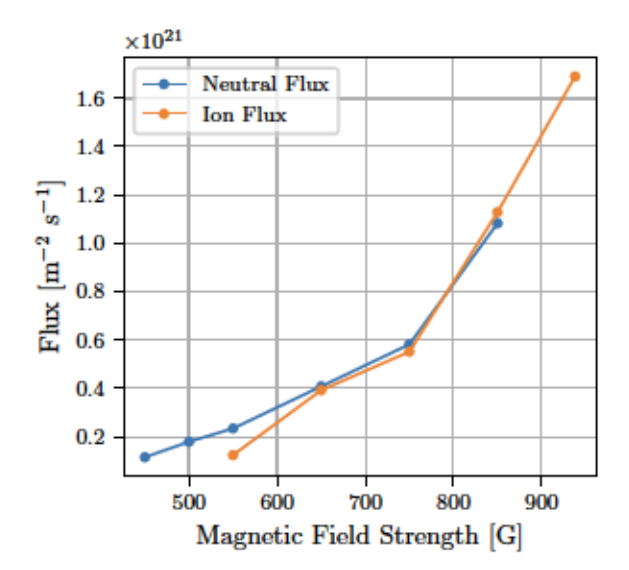


FIG. 10. Scaling  $n_0$  in Equation 4 by  $7.2 \times 10^{16}$  was sufficient to match the indident ion flux to the recycling neutral flux. The ion flux, shown by the orange curve, is from direct measurement. The neutral flux was inferred by fitting Equation 4 to the neutral argon LIF intensity data.

The level of agreement between the experimental neutral argon LIF data and the relatively simple model used to fit it adds confidence that the underlying physics are being captured to first order. Assuming this is true, the ionization rate can again be calculated as the neutral atom loss rate. In the model presented above, the atoms lost from the ground state population are step-wise excited and ionized. The ionization rate can thus be estimated by calculating the neutral ground state population loss rate. The loss rate can be calculated using the same model as Equation 3. The ionization rate is thus

$$S(z) = \frac{d(n_1V)}{dz} = V \frac{d(n_1)}{dz} = -V \lambda_1 n_1.$$
 (5)

Figure 11 shows the ionization rates calculated using Equation 5 and the data from Table I. For axial positions above 1250 mm, these ionization rates are comparable with those calculated from the ion LIF data. However, the ionization rates calculated from the neutral LIF data do not reflect the  $10^{22}$  m<sup>-3</sup>s<sup>-1</sup> ionization rates in the presheath region. The neutral ionization rates at axial locations below 1250 mm are significantly lower than the ion LIF data. This suggests that while ionization of axially recycling neutrals is likely still occuring, it is not a dominant source of ions in this region. The axial location of 1250 mm is therefore likely the transition point between axially dominant fueling and radially dominant fueling.

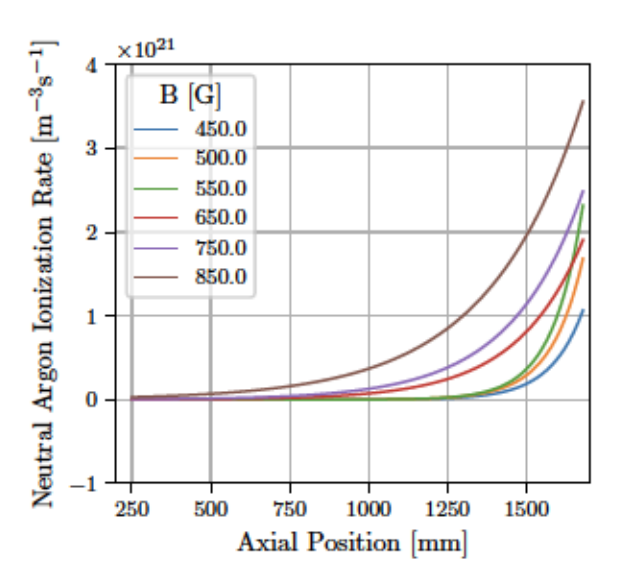


FIG. 11. Ionization rates calculated using Equation 5 and the data in Table I.

The radial LIF intensity and flow velocity was measured for neutral argon at the same locations as for the singly ionized argon case. The fluorescence intensity is shown in Figure 12 as a function of magnetic field strength. The intensity measured just beyond the antenna at 680 mm, shown in Figure 12A, is initially quite

high on axis and at low magnetic field strength. However, moving away from the axis, increasing the magnetic field strength, and moving further down stream substantially reduce the LIF intensity. For higher magnetic fields, where the electron density is greater, the lower neutral LIF intensity is a result of a lower neutral atom density.

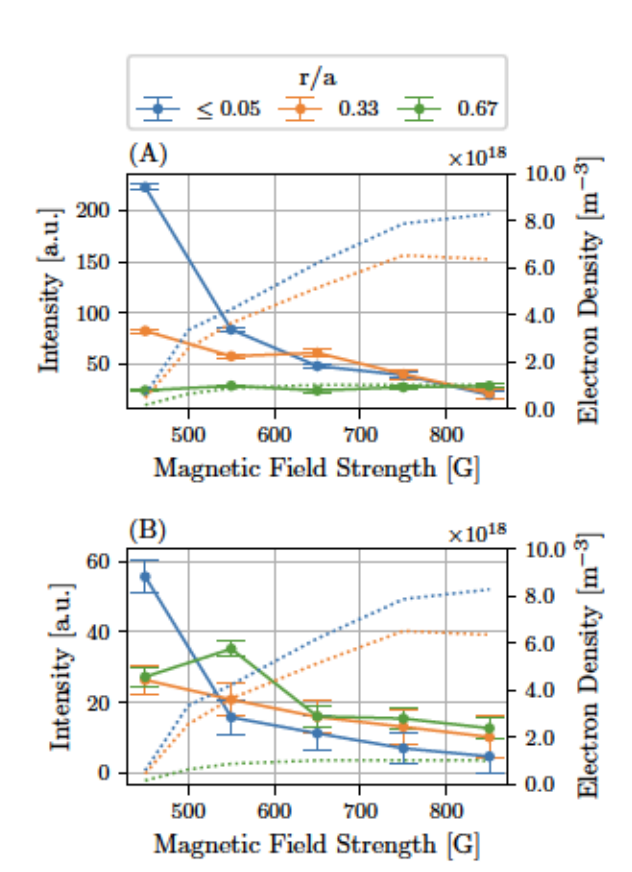


FIG. 12. Radial LIF intensity of neutral argon. A.) Data taken at 680 mm, just downstream of the antenna. B.) Data taken in front of the boundary plate. The LIF intensity is shown by the solid lines, the electron density measured by the Langmuir probe is shown by the dotted lines.

As with the argon ions, the radial flow of neutral argon atoms was measured with LIF. The radial flow velocity data is shown in Figure 13 at the same three radial locations as the ion data. At  $r/a \leq 0.05$  the flow velocity is nearly zero for all axial locations and magnetic field strengths. At r/a = 0.33 the radial flow velocity for all magnetic field strengths shift slightly negative (inward) for axial positions below 1200 mm. However, v = 0 is still within the uncertainty bars. For r/a = 2/3, the flow velocity is a bit more negative than at r/a = 1/3, and now v = 0 is not within the uncertainty. The increasingly inward flow velocity suggests radial fueling of the plasma is indeed taking place for axial positions between 210 mm and 1200 mm. For axial positions above 1500

mm, the radial flow velocity is not significantly dependent on magnetic field strength or radial position and tends to hover around -10 m/s.

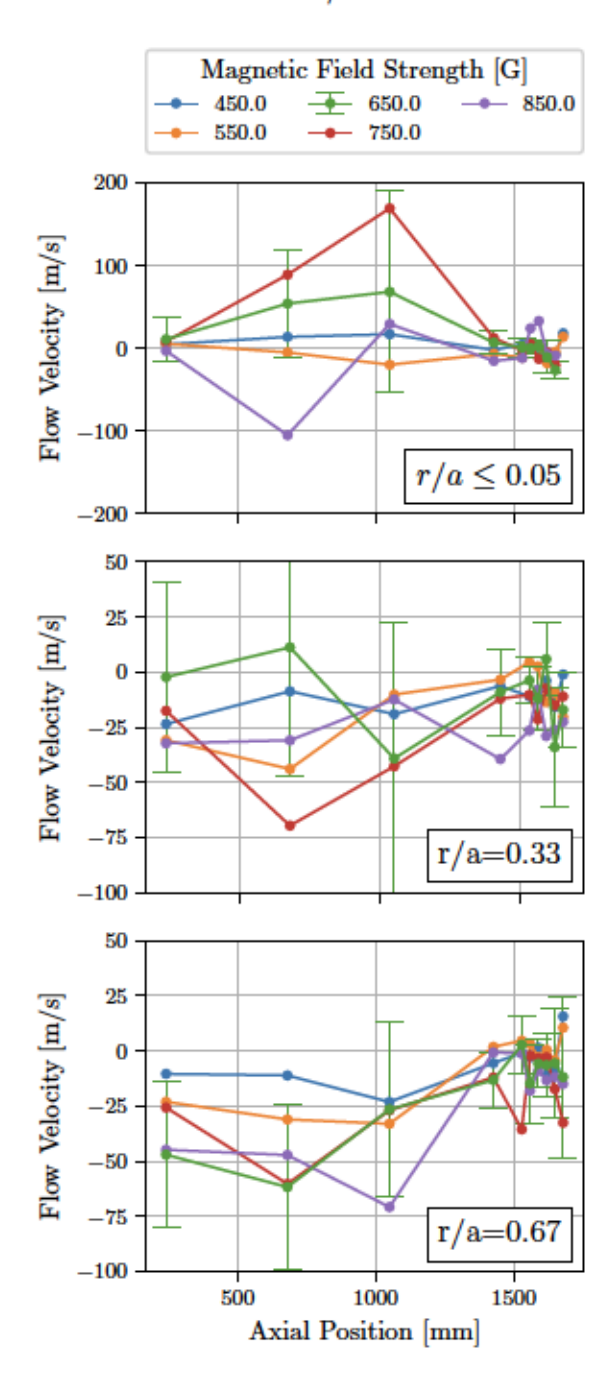


FIG. 13. Neutral argon LIF radial flow velocity measurements along the axis of MARIA. Errorbars on the 650 G trace are typical for magnetic field strength greater than 450 G. The data at  $r/a \leq 0.05$  is taken within 4 mm of the axis, but cannot be exactly on axis due uncertainty in radial positioning

Unfortunately the radial neutral LIF intensity cannot be converted into a neutral flux. In the axial case, the conservation of mass equation formed a strong relationship between the incident ion flux and the recycling neutral flux. The ability to take measurements very close to the boundary plate, and thus form a realistic control volume was essential to that analysis. In the radial case, refraction through the glass chamber wall and significantly reduced ion LIF intensity meant LIF measurements could not be taken right next to the chamber wall. A realistic control volume cannot therefore be defined to leverage conservation of mass in converting the neutral LIF intensity and velocity into a neutral flux estimate.

## V. DISCUSSION AND CONCLUSION

The flow measurements for neutral and singly ionized argon in both the axial and radial direction presented above begin to paint a picture of the particle balance in the MARIA helicon device. The flux of ions flowing along the axis of MARIA exhibits clear scaling with magnetic field strength and the greatest ion loss term was due to axial flux near the boundary plate. The radial ion flux of  $2.5-5\times10^{20}~\mathrm{m}^{-2}\mathrm{s}^{-1}$  between the antenna and the boundary plate is comparable to the axial flux in the same region. The ion loss due to axial flow is therefore dominant near the axial boundaries, but radial and axial ion loss is of similar magnitude throughout the bulk plasma.

The neutral LIF data indicates a substantial buildup of neutral atoms directly in front of the downstream chamber boundary. This buildup of neutral atoms necessarily has an impact on both the ion losses and the neutral fueling of the plasma. The apparent flow velocity reversal is one such impact and strongly suggests ion-neutral momentum exchange is occurring in that region. The radial neutral argon LIF data is less difinitive, but clearly indicates a depletion of neutral atoms at higher electron densities. The neutral argon radial flow velocity indicates an inward flow of neutral argon atoms between the antenna and downstream boundary plate, while the radial flow is essentially zero near the boundary plate.

Combining the ion and neutral argon LIF data suggests a kind of circulatory ionization and recycling process is taking place in MARIA. Ions produced just downstream of the antenna are lost radially and axially in approximately equal proportions. Ions lost in the radial direction are simply recycled after neutralizing on the chamber wall. Ions that continue along the axis possibly exchange momentum with a higher density cloud of neutral atoms before impinging on the axial boundary plate and neutralizing. The neutral atoms recycling off the plate encounter an intense flux of ions and electrons and are either immediately ionized and sent back towards the plate or make their way further upstream before eventually being ionized. This proposed sequence sets up a net flux of ions in the downstream direction and a net flux of neutrals in the upstream direction. The increased inward flow of neutral atoms in the bulk plasma region near the antenna suggests neutral atoms recycling off the axial boundary plate eventually rebound of the radial chamber

wall and join the flux of neutral atoms recycling radially.

It is important to note that this particular fueling cycle is likely unique to the chamber geometry on MARIA where the gas source and vacuum pump is located at the same upstream location of the chamber. Different gas source arrangements will likely result in very different flows, especially when the gas is sourced upstream and the vacuum pump is located downstream. The impact of these alternative vacuum arrangements, including the use of a large expansion chamber at the downstream location, on the plasma flows and ultimate density are the subject of future research.

#### **ACKNOWLEDGMENTS**

This work was funded by the National Science Foundation under NSF CAREER award PHY-1455210 and by funds of the Engineering Physics Department in the College of Engineering at the University of WisconsinMadison. The support and invaluable input and consultation of Prof Noah Hershkowitz on Helicon plasmas is greatly appreciated.

#### **REFERENCES**

- <sup>1</sup>B. Buttenschön, N. Fahrenkamp, and O. Grulke, "A high power, high density helicon discharge for the plasma wakefield accelerator experiment AWAKE," Plasma Physics and Controlled Fusion **60**, 075005 (2018).
- <sup>2</sup>P. Zhu and R. W. Boswell, "Ar ii laser generated by Landau damping of whistler waves at the lower hybrid frequency," Phys. Rev. Lett. **63**, 2805–2807 (1989).
- <sup>3</sup>A. W. Degeling, T. E. Sheridan, and R. W. Boswell, "Intense on-axis plasma production and associated relaxation oscillations in a large volume helicon source," Physics of Plasmas 6, 3664 (1999).

- <sup>4</sup>R. M. Magee, M. E. Galante, J. Carr, G. Lusk, D. W. McCarren, and E. E. Scime, "Neutral depletion and the helicon density limit," Physics of Plasmas **20**, 2–6 (2013).
- <sup>5</sup>F. F. Chen, "Physics of Helicon Discharges," Physics of Plasmas 3, 1783–2797 (1996).
- <sup>6</sup>E. Scime, R. Hardin, C. Biloiu, a. M. Keesee, and X. Sun, "Flow, flow shear, and related profiles in helicon plasmas," Physics of Plasmas 14, 043505 (2007).
- <sup>7</sup>R. M. Magee, M. E. Galante, N. Gulbrandsen, D. W. McCarren, and E. E. Scime, "Direct measurements of the ionization profile in krypton helicon plasmas," Physics of Plasmas 19, 123506 (2012).
- <sup>8</sup>J. Green and O. Schmitz, "Construction of a linear plasma device for studying helicon plasmas relevant to plasma wakefield accelerators," (2019).
- <sup>9</sup>F. F. Chen, "Langmuir probe measurements in the intense RF field of a helicon discharge," Plasma Sources Science and Technology **21**, 055013 (2012).
- <sup>10</sup>G. D. Severn, D. A. Edrich, and R. McWilliams, "Argon ion laser-induced fluorescence with diode lasers," Review of Scientific Instruments 69, 10 (1998).
- <sup>11</sup>J. Green, O. Schmitz, G. Severn, and V. Winters, "Exploiting Zeeman effect symmetries to measure particle velocities in magnetized plasmas," Measurement Science and Technology 30, 055202 (2019).
- <sup>12</sup>A. M. Keesee, E. E. Scime, and R. F. Boivin, "Laser-induced fluorescence measurements of three plasma species with a tunable diode laser," Review of Scientific Instruments 75, 4091–4093 (2004).
- <sup>13</sup>H.-J. Woo, K.-S. Chung, T. Lho, and R. Mcwilliams, "A Newly Calibrated Laser-Induced Fluorescence ( LIF ) System for Ar Ions with a Single Tunable Diode Laser," Journal of the Korean Physical Society 48, 260–265 (2006).
- <sup>14</sup>W. Whaling, W. Anderson, M. Carle, J. Brault, and H. Zarem, "Argon ion linelist and level energies in the hollow-cathode discharge," Journal of Quantitative Spectroscopy and Radiative Transfer 53, 1–22 (1995).
- <sup>15</sup>A. Kramida, Y. Ralchenko, J. Reader, and N. A. Team, "NIST Atomic Spectra Database (version 5.6.1)," (2018).
- <sup>16</sup>W. Whaling, W. H. C. Anderson, and M. T. Carle, "Argon I Lines Produced in a Hollow Cathode Source, 332 nm to 5865 nm," Journal of Research Of The National Institute of Standards and Technology 107, 149 169 (2002).
- <sup>17</sup>P. Stangeby, The Plasma Boundary of Magnetic Fusion Devices (Institute of Physics Publishing, 2000) publication Title: Plasma Physics and Controlled Fusion.
- <sup>18</sup>J. Rapp, L. W. Owen, J. Canik, J. D. Lore, J. F. Caneses, N. Kafle, H. Ray, and M. Showers, "Radial Transport Modeling of High Density Deuterium Plasmas in Proto-MPEX with the B2.5-Eirene Code," Physics of Plasmas 26, 042513 (2019).